



**HAL**  
open science

## **A novel multisite confocal system for rapid Ca<sup>2+</sup> imaging from submicron structures in brain slices**

Luiza Filipis, Karima Ait Ouares, Philippe Moreau, Dimitrii Tanese, Valeria Zampini, Andrea Latini, Chun X. Bleau, Charlie Bleau, Jeremy Graham, Karima Ait Ouares, et al.

### ► **To cite this version:**

Luiza Filipis, Karima Ait Ouares, Philippe Moreau, Dimitrii Tanese, Valeria Zampini, et al.. A novel multisite confocal system for rapid Ca<sup>2+</sup> imaging from submicron structures in brain slices. *Journal of Biophotonics*, 2018, 11 (3), <10.1002/jbio.201700197>. <hal-01872699>

**HAL Id: hal-01872699**

**<https://hal.science/hal-01872699v1>**

Submitted on 12 Sep 2018

**HAL** is a multi-disciplinary open access archive for the deposit and dissemination of scientific research documents, whether they are published or not. The documents may come from teaching and research institutions in France or abroad, or from public or private research centers.

L'archive ouverte pluridisciplinaire **HAL**, est destinée au dépôt et à la diffusion de documents scientifiques de niveau recherche, publiés ou non, émanant des établissements d'enseignement et de recherche français ou étrangers, des laboratoires publics ou privés.



HAL Authorization

Article type: Original Paper

**A novel multisite confocal system for rapid Ca<sup>2+</sup> imaging from  
submicron structures in brain slices**

*Luiza Filipis<sup>1,2</sup>, Karima Ait Ouares<sup>1,2</sup>, Philippe Moreau<sup>1</sup>, Dimitrii Tanese<sup>3</sup>, Valeria  
Zampini<sup>3</sup>, Andrea Latini<sup>4</sup>, Chun Bleau<sup>5</sup>, Charlie Bleau<sup>6</sup>, Jeremy Graham<sup>7</sup>, Marco  
Canepari<sup>1,2,8,\*</sup>*

\*Corresponding Author: E-mail: marco.canepari@univ-grenoble-alpes.fr

<sup>1</sup>Laboratory for Interdisciplinary Physics, UMR 5588 CNRS and Université Grenoble  
Alpes and, 38402 Saint Martin d'Hères, France.

<sup>2</sup>Laboratories of Excellence, Ion Channel Science and Therapeutics, France.

<sup>3</sup>Wavefront-Engineering Microscopy Group, Neurophotonics Laboratory, UMR8250  
CNRS and Paris Descartes University, Paris, France.

<sup>4</sup>CrestOptics Spa, 00167 Rome, Italy

<sup>5</sup>RedshirtImaging LLC, Decatur, GA30030, USA

<sup>6</sup>SciMeasure Analytical Systems Inc, Decatur, GA 30030, USA

<sup>7</sup>Cairn Research Ltd, Faversham ME13 8UP, United Kingdom

<sup>8</sup>Institut National de la Santé et Recherche Médicale (INSERM), France.

Keywords: confocal microscopy, calcium imaging, neurons, brain slices

**Abstract**

In brain slices, resolving fast  $\text{Ca}^{2+}$  fluorescence signals from submicron structures is typically achieved using two-photon or confocal scanning microscopy, an approach that limits the number of scanned points. The novel multiplexing confocal system presented here overcomes this limitation. This system is based on a fast spinning disk, a multimode diode laser and a novel high-resolution CMOS camera. The spinning disk, running at 20,000 rpm, has custom-designed spiral pattern that maximises light collection while rejecting out-of-focus fluorescence to resolve signals from small neuronal compartments. Using a 60X objective, the camera permits acquisitions of tens of thousands of pixels at resolutions of  $\sim 250$  nm per pixel in the kHz range with 14 bits of digital depth. The system can resolve physiological  $\text{Ca}^{2+}$  transients from submicron structures at 20-40  $\mu\text{m}$  below the slice surface, using the low affinity  $\text{Ca}^{2+}$  indicator Oregon Green BAPTA-5N. In particular, signals at 0.25-1.25 kHz were resolved in single trials, or through averages of a few recordings, from dendritic spines and small parent dendrites in cerebellar Purkinje neurons. Thanks to an unprecedented combination of temporal and spatial resolution with relatively simple implementation, it is expected that this system will be widely adopted for multisite monitoring of  $\text{Ca}^{2+}$  signals.

**1. Introduction**

$\text{Ca}^{2+}$  fluorescence imaging allows the detailed investigation of biochemical processes that are triggered by transient elevation of intracellular  $\text{Ca}^{2+}$ . In particular,  $\text{Ca}^{2+}$  transients can be recorded from individual neurons in brain slices to investigate local mechanisms of physiological importance.[1] In these recordings, the number of detected photons necessary to resolve fluorescence changes with adequate signal-to-noise ratio (S/N)

determines the dimension of emitting sites or the duration of exposure time-window.[2] Hence, at a given acquisition rate, the smallest useful detection element is the one from which the number of emitted photons allows the signal to be above the photon (shot) noise. Detection of fluorescence changes from structures  $\leq 1 \mu\text{m}$  at temporal resolution of  $\sim 1 \text{ ms}$  is satisfactory for investigating many physiological signals from relevant neuronal compartments in dendrites and axons. In addition, it is also crucial to monitor  $\text{Ca}^{2+}$  signals from many sites simultaneously. The most straightforward methodology involves uniformly illuminating the whole area of interest and recording  $\text{Ca}^{2+}$  fluorescence with a fast camera (widefield imaging). In widefield imaging, the lateral resolution limit is theoretically given by  $1.22 \cdot \lambda_{\text{em}}/\text{NA}$ , where NA is the numerical aperture of the objective used and  $\lambda_{\text{em}}$  is the fluorescence emission wavelength.[3] Thus, objectives with  $\text{NA} \geq 1$  can ideally resolve signals from structures  $\leq 1 \mu\text{m}$  at all visible wavelengths. This theoretical resolution limit is however compromised for fluorescence signals originating from structures in brain slices that are tens of microns below the slice surface. In this case, the tissue between the fluorescence-emitting structure and the slice surface scatters light decreasing spatial resolution and preventing the possibility of resolving signals from submicron structures.[4] A way to recover the original spatial resolution is to reject tissue scattered photons by mean of confocal microscopy.[5] Conventional confocal microscopy, performed by scanning a pinhole and recording fluorescence with a photomultiplier, can work at high acquisition rates by limiting the capture to line-scans or random-access scans.[6] In this approach, however, the exposure time and therefore the number of photons recorded in each point is inversely proportional to the number of scanned points. Thus, the number of photons necessary to provide the adequate S/N limits the number of scanned points or the sampling rate. One way to overcome these limitations is to use a spinning disk.[7] A rapidly spinning disk is positioned conjugate with the focal plane in

both illumination and detection pathways to scan a series of transparent pinholes over the field of view of a digital camera. This fast parallel-scan approach significantly reduces the instantaneous photon dose required and increases the acquisition rate. Using this approach, several systems were recently implemented for  $\text{Ca}^{2+}$  imaging in various preparations.[7-10] In this article, we report the design and the assessment of a novel confocal system, based on a spinning disk specifically designed for rapid  $\text{Ca}^{2+}$  imaging from submicron structures in brain slices. The pinhole array pattern was replaced with a spiral pattern that maximises emitted light detection while preserving the resolution in the order of the diffraction limit (see Materials and Methods). The high fluorescence excitation is obtained using a 1.2 W laser coupled to the spinning disk, with light detection at high spatial and temporal resolution achieved using a fast CMOS camera.

## 2. Materials and methods

### 2.1. Slice preparation, solutions and electrophysiology

Experiments were ethically carried out in accordance with European Directives 2010/63/UE on the care, welfare and treatment of animals. Procedures were reviewed by the ethics committee affiliated to the animal facility of the university (D3842110001). Transversal hippocampal and cerebellar sagittal slices (250  $\mu\text{m}$  thick) were prepared from 21-35 postnatal days old mice (C57Bl6) following established procedures [11-12] with a Leica VT1200 (Leica, Wetzlar, Germany) and incubated at 37°C for 1 hour before use. The extracellular solution contained (in mM): 125 NaCl, 26  $\text{NaHCO}_3$ , 1  $\text{MgSO}_4$ , 3 KCl, 1  $\text{NaH}_2\text{PO}_4$ , 2  $\text{CaCl}_2$  and 20 glucose, bubbled with 95%  $\text{O}_2$  and 5%  $\text{CO}_2$ . The intracellular solution contained (in mM): 125  $\text{KMeSO}_4$ , 5 KCl, 8  $\text{MgSO}_4$ , 5  $\text{Na}_2\text{-ATP}$ ,

0.3 Tris-GTP, 12 Tris-Phosphocreatine, 20 HEPES, adjusted to pH 7.35 with KOH. The  $\text{Ca}^{2+}$  indicator Oregon Green BAPTA-5N (OG5N,  $K_D=35\mu\text{M}$ ) was added to the internal solution at 2 mM. Patch-clamp recordings were made at 32-34°C using a Multiclamp amplifier 700A (Molecular Devices, Sunnyvale, CA) and signals acquired at 20 kHz using a USB-6221 board (National Instruments, Austin, TX). The measured membrane potential was corrected for junction potential (-11 mV) as previously estimated[13]. In experiments on cerebellar Purkinje neurons (PNs), either climbing fibre (CF) or parallel fibre (PF) excitatory postsynaptic potentials (EPSPs), were elicited by current pulses, of 5-20  $\mu\text{A}$  amplitude and 100  $\mu\text{s}$  duration delivered by a pipette. In experiments on CA1 hippocampal pyramidal neurons, action potentials were elicited by 2 ms current pulses through the patch pipette.

## 2.2. Detailed description of the confocal system

The system was mounted on a SliceScope microscope (Scientifica, Uckfield, UK) equipped with motorised XY translation stage, PatchStar manipulators and 60X Olympus water immersion objective (NA=1). The motorised Z translation allowed estimation of the depth of the recording plane from the slice surface. The microscope incorporated an OptoLED unit (Cairn Research, Faversham, UK) mounted on the Olympus epifluorescence unit to provide widefield illumination at 470 nm independent of the spinning disk. The system, illustrated in the scheme of **Figure 1(A)**, is based on two units: 1. the spinning disk unit and 2. the CMOS camera.

### 2.2.1. Spinning disk unit

The spinning disk is a customised version of the X-Light, developed by CrestOptics Spa (Rome, Italy). This incorporates a disk which, instead of pinholes, has multiple sets of continuous spirals with the following structure: (a) 36 spirals; (b) spiral thickness of 90

$\mu\text{m}$ ; (c) spiral step of 16.2 mm; (d) spiral-to-spiral radial distance of 450  $\mu\text{m}$  (**Figure 1(B)**). The disk was installed in the primary image plane of the microscope. The spiral pattern was projected to the sample to scan the entire field of view 36 times per disk revolution. The modified disk unit was run at 20,000 rpm (333,33 revolution per second). Finally, the spinning disk was automated to move in and out of the light path to enable both confocal and widefield imaging in the same experiment. The spinning disk was coupled to a TriLine LaserBank (Cairn Research) through a  $\text{\O}550 \mu\text{m}$ , 0.22 NA, SMA-SMA Fiber patch cable (Thorlabs, Newton, NJ). The laser head used was a multimode diode 465nm/1.2W (Ushio). A custom 25 mm focal length aspheric condenser (Cairn Research) was used at the output of the fibre to generate a concentrated and homogeneous illumination field of  $\sim 60 \mu\text{m}$  at the sample (**Figure 1(C)**). The fibre was stressed and vibrated to mix modes to reduce laser speckle and improve homogeneity. Finally, the whole confocal system was tested for optical sectioning performance against widefield illumination using 500 nm fluorescent beads attached to a coverslip (**Figure 1(D)**) and taking images at different depths below the focal plane of the bead with steps of 250 nm (comparable to the pixel dimension). In  $N = 16$  beads, fluorescence normalised to the value in the focal plane was  $0.68 \pm 0.09$ ,  $0.28 \pm 0.09$  and  $0.10 \pm 0.02$  at 1  $\mu\text{m}$ , 2  $\mu\text{m}$  and 3  $\mu\text{m}$  respectively in confocal imaging. These values were significantly different from  $0.86 \pm 0.04$ ,  $0.51 \pm 0.10$  and  $0.22 \pm 0.12$  obtained in widefield imaging ( $p < 0.001$ , paired t-test), indicating a clear improvement in optical sectioning in confocal imaging.

### 2.2.2. CMOS camera

The camera is a DaVinci-2K (SciMeasure, Decatur, GA) which uses a low-noise 2k by 2k pixel CMOS sensor with traditional readout architecture and true on-chip binning. The flexible sensor and camera design allows low read-noise performance ( $< 2.8e^-$ ) using either correlated double sampling (CDS) or non-destructive read (NDR) to subtract the

reset voltage. The large pixel size of  $15\mu\text{m}\times 15\mu\text{m}$  gives a relatively high fill-factor and hence a native quantum efficiency of 65% without requiring microlenses. A single 14-bit A/D per readout channel is used to achieve high bit depth without the dual-amplifier stitching required in sCMOS cameras. 16 parallel readout channels are implemented to achieve high frame rates without compromising noise. This is the first use of this novel camera in CDS mode for high speed live-cell imaging, although an alternative configuration has been used for stochastic super resolution of fixed samples using NDR.[14] Within the present configuration, each pixel is mapped to collect light from a square of  $\sim 250$  nm side. Data were acquired using Turbo-SM written in C by RedShirtImaging (Decatur, GA).

### *2.3. Optical recordings and analysis*

Laser or LED Fluorescence excitation, was band-passed filtered at  $469\pm 17$  nm (Semrock, Rochester, NY) and reflected towards the objective by a 495 nm longpass dichroic mirror (Chroma, Bellows Falls, VT). Emitted OG5N fluorescence was filtered at  $525\pm 25$  nm (Chroma) before detection. Synchronisation of the camera with laser and LED illumination and with the electrophysiology was provided by a Master 9 (A.M.P.I., Jerusalem, Israel). The timing of synaptic stimulation or action potentials was set during the acquisition window to prevent jittering when averaging over 3-9 trials. Fluorescence signals were sometimes corrected for bleaching by subtraction of filtered trials without signal. Fluorescence signals were expressed as fractional changes of fluorescence ( $\Delta F/F_0$ ).

## **3. Results**

In the Results section we describe the temporal and the spatial performances of the system and we present two examples of measurements that can be achieved.

### 3.1. Temporal performance of the system

The temporal performance of the system relies on the characteristics of the CMOS, illustrated in the picture of **Figure 2(A)**. The sensor ( $\sim 3\text{cm} \times 3\text{cm}$ ), is composed of  $2048 \times 2048$  pixels. As depicted in **Figure 2(A)**, the full-frame image array is divided into 16 rectangular  $256 \times 1024$  pixel arrays processed in parallel. In our configuration, however, the field of view of the image covers around half of the sensor length, reducing the size of the acquired array to  $1024 \times 1024$  pixels. The left image of **Figure 2(B)** shows the dendrite of a PN filled with 2 mM OG5N. This image was collected without the spinning disk in place using widefield LED illumination. The image on the right was recorded using laser illumination with the spinning disk. The maximal acquisition rate of the camera depends on the vertical dimension of the acquired pixel array. In the right image of **Figure 2(B)**, several acquired arrays are outlined by coloured rectangles:  $1024 \times 1024$  pixels (blue, maximal rate 200 frames/s);  $1024 \times 512$  pixels (green, maximal rate 400 frames/s);  $1024 \times 256$  pixels (red, maximal rate 800 frames/s);  $1024 \times 160$  pixels (purple, maximal rate 1250 frames/s). **Figure 2(C)** shows a portion of the dendrite captured with the LED (left) or with the laser and the spinning disk (right). The coloured traces on the bottom of **Figure 2(C)** are the  $\Delta F/F_0$  signals, averaged over the  $40 \times 40$  pixels region shown with a yellow square on the right image of **Figure 2(C)**, acquired at the maximal acquisition rates in single trials. These signals associated with a CF-EPSP illustrate generically the excellent quality of the signal at acquisition rates up to more than 1 kHz. The images in **Figure 2(D)** show a portion of the dendrite in panel (C). Three regions of  $2 \times 2$  pixels ( $\sim 0.25 \mu\text{m}^2$ ) from where fluorescence was averaged are indicated:

1 and 3 corresponding to two individual synaptic spines and 2 corresponding to the bulk of the parent dendrite. Traces on the right report the corresponding  $\Delta F/F_0$  signals at 1250 Hz, associated with a CF-EPSP, obtained by averaging three trials. In summary, these recordings demonstrate that our confocal system is capable of recording  $\text{Ca}^{2+}$  signals, from structures  $< 1 \mu\text{m}$ , at frame intervals  $< 1 \text{ms}$ .

### 3.2. Spatial performance of the system

The spatial performance was assessed by analysing fluorescence profiles and transients in sequential recordings without or with the spinning disk (widefield vs confocal imaging). A first assessment was carried out in the initial part of apical dendrites from CA1 hippocampal pyramidal neurons, an approximately cylindrical structure. In **Figure 3(A)**, images of three dendrites at 23, 37 and 50  $\mu\text{m}$  depth from the slice surface ( $\delta$ ) were obtained in widefield (*wf*) or confocal (*sd*) imaging. The X-line is positioned on the site of the dendrite in focus and the absolute intensity profile in **Figure 3(B)** was calculated by averaging fluorescence from  $2 \times 4$  pixels regions and normalising the values to the maximum at  $X=0$ . The profile was fitted with a Lorentzian function

$$\frac{1}{\pi} \cdot \frac{\Gamma/2}{X^2 + (\frac{\Gamma}{2})^2} \quad (1).$$

The parameter  $\Gamma$  specifies the width of the intensity profile that depends on the dendrite thickness, but also on light scattering [15] and it is systematically larger in widefield imaging ( $\Gamma_{wf}$ ) with respect to spinning disk imaging ( $\Gamma_{sd}$ ), as shown in Figure 3(B). We then computed  $\Delta F/F_0$  associated with four action potentials at  $X=\pm\Gamma_{sd}$  for widefield and confocal imaging and normalised the signals to those at  $X=0$ . As shown in the plots on the right of panel (B), the  $\Delta F/F_0$  at  $\pm\Gamma_{sd}$  was systematically smaller in confocal imaging. **Figure 3(C)** reports the analysis of intensity profiles from 8 dendrites in 5 cells.  $\Gamma$  values in widefield and confocal imaging, as well as their difference ( $\Gamma_{wf}-\Gamma_{sd}$ ), increase with  $\delta$ .

Whereas  $\Gamma_{wf}$  and  $\Gamma_{sd}$  also depend on the dendrite thickness,  $\Gamma_{wf}/\Gamma_{sd}$  is expected to depend only on tissue scattering, providing an estimate of the improvement produced by the spinning disk. Thus, at  $\pm\Gamma_{sd}$ , the normalised  $\Delta F/F_0$  peak assesses the ability of the system to resolve  $\text{Ca}^{2+}$  transients free of scattered light. **Figure 3(D)** reports the mean $\pm$ SD of normalised  $\Delta F/F_0$  peak at  $\pm\Gamma_{sd}$ , that was  $0.27\pm 0.07$  in confocal imaging, significantly smaller than  $0.55\pm 0.17$  in widefield imaging ( $p < 0.001$ , paired t-test). In summary, within  $40\ \mu\text{m}$  from the surface, the gain in spatial resolution quantified by  $\Gamma_{wf}/\Gamma_{sd}$  was between  $200$  and  $600\ \text{nm}$ . This result can be interpreted as an indication that, within  $40\ \mu\text{m}$  from the slice surface, our system can de-blur images to restore spatial resolution closer to the diffraction limit. Hence, in this  $\delta$  range, we assessed the ability of the system to resolve signals from submicron structures by measuring  $\Delta F/F_0$  associated with CF-EPSPs from PN synaptic spines. **Figure 4(A)** shows widefield (*wf*) and confocal images (*sd*) of a PN dendrite at  $\delta = 25\ \mu\text{m}$ . Fluorescence was averaged over two regions of  $2 \times 2$  pixels centred onto two spines in focus, and on regions at  $\sim 0.5\ \mu\text{m}$  and  $\sim 1\ \mu\text{m}$  from the edge of the spine-centred regions outside the cell. **Figure 4(B)** shows that, in widefield imaging,  $\Delta F/F_0$  signals are comparable in size in spines and in the adjacent regions outside the cell. In contrast, in confocal imaging, the  $\Delta F/F_0$  signals were progressively smaller with the distance from the spine, indicating scattered light elimination by the spinning disk. The same analysis was done in 48 spines in focus from six cells, with varying  $\delta$  from  $18\ \mu\text{m}$  to  $30\ \mu\text{m}$ . **Figure 4(C)** reports the mean $\pm$ SD of  $\Delta F/F_0$  peaks at  $\sim 0.5\ \mu\text{m}$  and  $\sim 1\ \mu\text{m}$  distance from the cell, normalised to the peaks on the spine centres, in widefield and confocal imaging. In confocal imaging, the normalised peaks at  $\sim 0.5\ \mu\text{m}$  and  $\sim 1\ \mu\text{m}$  distance were  $0.62\pm 0.11$  and  $0.29\pm 0.08$  respectively, significantly smaller than  $0.90\pm 0.13$  and  $0.86\pm 0.16$  respectively in widefield imaging ( $p < 0.001$ , paired t-test). In particular, the  $\sim 0.3$  value at  $\sim 1\ \mu\text{m}$  distance in confocal imaging, is within our ability to discriminate the

signal from noise as shown in the examples of **Figure 4(B)**. This indicates that we can resolve  $\text{Ca}^{2+}$  signals from submicron structures in this  $\delta$  range where this task cannot be accomplished by widefield imaging. Another advantage of confocal imaging, with respect to widefield imaging, is the reduced bleaching. Dendrite of **Figure 5(A)** was exposed to laser illumination for 80 ms with the spinning disk at the maximal intensity, or without the spinning disk at reduced intensity to obtain a similar photon noise. As shown in the plots of **Figure 5(B)**, dye bleaching reduced fluorescence by ~3 % in widefield imaging, but only by ~0.5 % in confocal imaging. In 7 cells tested, bleaching was  $2.9 \pm 1.0$  % in widefield imaging, significantly larger than in spinning disk imaging ( $0.5 \pm 0.1$  %,  $p < 0.001$  paired t-test).

### 3.3. Examples

After evaluating the system, we describe two examples of the type of information accessible with this approach. In the cell of **Figure 6(A)**, the  $\text{Ca}^{2+}$  signal associated with the CF-EPSP was recorded at 500 Hz in two areas containing several dendritic branches and many spines. Such recordings permit exhaustive analysis of the amplitude and kinetics of  $\text{Ca}^{2+}$  transients in synaptic spines with respect to those in parent dendrites. **Figure 6(B)** shows  $\text{Ca}^{2+}$  signals in four spines and four locations of the parent dendrites in the red and blue regions indicated in panel (A). These representative  $\Delta F/F_0$  signals indicate that the kinetics of the  $\text{Ca}^{2+}$  transient is systematically different in spines and parent dendrites. In particular,  $\text{Ca}^{2+}$  signals in spines are larger and decay more rapidly with respect to those in parent dendrites. This phenomenon may be due to the different surface-to-volume ratio of the two types of structure [16], as well as to different distributions of  $\text{Ca}^{2+}$  channels [17] or to  $\text{Ca}^{2+}$  binding proteins.[18] In the example of **Figure 7(A)**, we monitored the  $\text{Ca}^{2+}$  signal associated with PF-EPSPs. For this signal,

produced by activation of synaptic spines, the size and the extent of the  $\text{Ca}^{2+}$  transient depends on the number and spatial distribution of activated PFs.[20] In this example, the train of five EPSPs produced a  $\text{Ca}^{2+}$  transient in the dendrites and spines over a region of  $\sim 100 \mu\text{m}^2$ . As shown in **Figure 7(B)**, the  $\text{Ca}^{2+}$  signal had two components: a fast component nearly synchronous with the EPSPs recorded in the soma mediated by voltage-gated  $\text{Ca}^{2+}$  channels [20]; and a slower component mediated by metabotropic glutamate receptors.[21] The false-colour scale images in **Figure 7(C)** illustrate the spatial profile of the signal at different time-windows of the recording; in particular images *b* and *d* correspond to the peak of the fast and slow components. As shown by these images and by the traces in panel (B), the two signals do not spatially overlap. In some dendrites or spines the fast component was larger than the slow component and in other sites it was the opposite. This result suggests that activation of metabotropic glutamate receptors does not spatially coincide with activation of voltage-gated  $\text{Ca}^{2+}$  channels, i.e. that PF-EPSPs may trigger different signalling pathways at different sites of the dendrite. The two examples in Figure 5 and 6 demonstrate the advantages of our system with respect to scanning systems where only limited numbers of selected submicron sites can be simultaneously analysed. Movies of these experiments are available online (MovieS1 and MovieS2).

#### 4. Discussion and conclusions

The understanding of fast  $\text{Ca}^{2+}$  signaling in small axonal or dendritic compartments and in synaptic spines is crucial in neurobiology.[22] In this article, we report a novel fast confocal system based on a spinning disk specifically designed to investigate  $\text{Ca}^{2+}$  signals

in submicron neuronal compartments in brain slices, in combination with patch clamp recordings.[23] To this purpose, other confocal solutions have been proposed in the past few years. A scanning confocal imaging system developed for this application and based on pinholes and digital micromirror devices could operate in the kHz range, but was limited in the number of recording points.[24] Similarly, the number of recording points could be effectively increased by using fixed pinholes arrays.[25] but this approach limits the exact selection of recording sites. The confocal system described in this report overcomes these limitations allowing recording of  $\text{Ca}^{2+}$  transients from continuous structures in tens of thousands of pixels simultaneously. The system performs optimally in the common situation of structures at 20-40  $\mu\text{m}$  below the slice surface, where widefield illumination fails discriminating signals with submicron resolution. Under these conditions, we achieved recordings at 250-1250 Hz from submicron structures. This was possible thanks to the combination of a fast custom-patterned disk, an efficient powerful laser and a fast and sensitive CMOS camera. The acquisition rate of these recordings is sufficient to detect fast  $\text{Ca}^{2+}$  transients associated with action potentials or synaptic activity, although still insufficient to measure the kinetics of fast  $\text{Ca}^{2+}$  channels.[26-29] The limitation of confocal imaging in acquisition speed is mainly set by the number of detected photons, which is reduced by light rejection. The way to obtain submicron resolution without rejection of emitted light is to use two-photon imaging that also allows axial confinement of fluorescence excitation.[30] Two-photon imaging without scanning microscopy is achievable by patterning the light shape to match the imaged structures, i.e. by performing two-photon holographic illumination.[31] In voltage imaging, signals have been recorded at several kHz from small neuronal compartments using one-photon holographic illumination.[32-33] In contrast, two-photon holographic illumination has been set for  $\text{Ca}^{2+}$  imaging in brain slices and in vivo, but without achieving recordings

from submicron structures in the kHz range.[34-37] Yet, it appears possible to achieve this resolution in the near future.

Whereas holographic two-photon imaging is potentially more powerful, the present confocal system has several advantages. It can be easily coupled to existing microscopes equipped for electrophysiology; it requires moderate knowledge of optics to implement measurements; it is economic requiring minimal maintenance. In particular, the multimode laser box allows other wavelengths for excitation of different indicators and is 5-10 times cheaper than lasers used in conventional confocal microscopes for equivalent power. Thus, this system offers an easy solution to measure fast  $\text{Ca}^{2+}$  transients in brain slices with submicron resolution.

## 5. Supporting Information

MovieS1: Example of spatial profile of  $\text{Ca}^{2+}$  signal associated with one CF-EPSP.

MovieS2: Example of spatial profile of  $\text{Ca}^{2+}$  signal associated with a train of PF-EPSPs.

## Acknowledgements

This work was supported by the *Agence Nationale de la Recherche* through: 1. Grant *WaveFrontImag*, program number ANR-14-CE17-0006-01; 2. Labex *Ion Channels Science and Therapeutics*, program number ANR-11-LABX-0015; 3. National Infrastructure France Life Imaging “Noeud Grenoblois” ; and by the *Federation pour la recherché sur le Cerveau* (FRC) through the grant *Espoir en tête* (in partnership with Rotary France). We thank Hanen Ziri for starting development of the software, Vanni Petrolli for preparing the beads and Irène Wang for useful discussions.

## References

- [1] F. Helmchen, K. Imoto, and B. Sakmann, *Biophys. J.* **70**, 1069–1081 (1996).
- [2] R. Davies, J. Graham, and M. Canepari, *J. Microsc.* **251**, 5–13 (2013).
- [3] G.H. Patterson, *Semin Cell Dev Biol.* **20**, 886–893 (2009).
- [4] Z.F. Mainen, M. Maletic-Savatic, S.H. Shi, Y. Hayashi, R. Malinow, and K. Svoboda, *Methods* **18**, 231–239 (1999).
- [5] A. Fine, W.B. Amos, R.M. Durbin, and P.A. McNaughton, *Trends Neurosci.* **11**, 346–351 (1988).
- [6] P. Saggau, *Curr. Opin. Neurobiol.* **16**, 543–550 (2006).
- [7] C.G. Coates, D.J. Denvir, N.G. McHale, K.D. Thornbury, and M.A. Hollywood, *J. Biomed. Opt.* **9**, 1244–1252 (2004).
- [8] Y. Takahara, N. Matsuki, Y. Ikegaya. *J. Integr. Neurosci.* **10**, 121–129 (2011).
- [9] F. Ceriani, C.D. Ciubotaru, M., Bortolozzi, and F.Mammano, *Methods Mol. Biol.* **1427**, 223–241 (2016).
- [10] J.P. Nguyen, F.B. Shipley, A.N. Linder, G.S. Plummer, M. Liu, S.U. Setru, J.W. Shaevitz, and A.M. Leifer, *Proc. Natl. Acad. Sci. USA* **113**, E1074–1081 (2016).
- [11] K.E. Vogt, S. Gerharz, J. Graham, and M. Canepari, *J. Physiol.* **589**, 489–494 (2011).
- [12] K.E. Vogt, S. Gerharz, J. Graham, and M. Canepari, *PLoS ONE*, **6**, e24911 (2011).
- [13] M. Canepari, S. Willadt, D. Zecevic D and K.E. Vogt, *Biophys. J.* **98**, 2032–2040 (2010).

- [14] S.F. Barnett, M. Snape, C.N. Hunter, M.A. Juárez, and A.J. Cadby, *Sci. Rep.* **7**, 42313 (2017).
- [15] T.R. Corle, C.H. Chou, and G.S. Kino, *Opt. Lett.* **11**, 770-772 (1986).
- [16] M. Canepari, and F. Mammano, *J. Neurosci. Methods* **87**, 1-11 (1999).
- [17] P. Isope, M.E. Hildebrand, and T.P. Snutch, *Cerebellum* **11**, 651-665 (2012).
- [18] H. Schmidt, K.M. Stiefel, P. Racay, B. Schwaller, and J. Eilers J, *J. Physiol.* **551**, 13-32 (2003).
- [19] K. Vogt, and M. Canepari, *Cerebellum* **9**, 284-290 (2010).
- [20] M. Canepari, and K. Vogt, *PLoS ONE* **3**, e4011 (2008).
- [21] M. Canepari, and D. Ogden, *J. Physiol.* **573**, 65-82 (2006).
- [22] C. Grienberger, and A. Konnerth, *Neuron* **73**, 862-885 (2012).
- [23] G.J. Augustine, *J. Neurosci. Methods* **54**, 163-169 (1994).
- [24] V. Bansal , S. Patel, and P. Saggau, *J. Biomed. Opt.* **11**: 34003 (2006).
- [25] T Tominaga, and Y. Tominaga, *J. Neurophysiol.* **110**, 553-561 (2013).
- [26] N. Jaafari, M. De Waard, M, and M. Canepari, *Biophys. J.* **107**, 1280–1288 (2014).
- [27] N. Jaafari, E. Marret, and M. Canepari, *Neurophotonics* **2**, 021010 (2015).
- [28] N. Jaafari, and M. Canepari, *J. Physiol.* **594**, 967–983 (2016).
- [29] K. Ait Ouares, N. Jaafari, and M. Canepari, *J. Neurosci. Methods* **268**, 66–77 (2016).
- [30] T.G. Oertner, *Exp. Physiol.* **87**, 733-736 (2002).
- [31] E. Papagiakoumou, A. Bégue, B. Leshem, O. Schwartz, B.M. Stell, J. Bradley, D. Oron, and V. Emiliani (2013), Functional patterned multiphoton excitation deep inside scattering tissue. *Nat. Photon.* **7**, 274-278 (2013).
- [32] A.J. Foust, V. Zampini, D. Tanese, E. Papagiakoumou, and V. Emiliani. *Neurophotonics* **2**, 021007 (2015).

- [33] D. Tanese, J.Y. Weng, V. Zampini, V. De Sars, M. Canepari, B. Rozsa, V. Emiliani, and Zecevic D. *Neurophotonics*, **4**, (2017).
- [34] V. Nikolenko, B.O. Watson, R. Araya, A. Woodruff, D.S. Peterka, and R. Yuste. *Front. Neural Circuits*. **2**, 5 (2008).
- [35] P. Pozzi , D. Gandolfi , M. Tognolina, G.J.E.Chirico, Mapelli, and E. D'Angelo, *Neurophotonics* **2**, 015005 (2015).
- [36] W. Yang, J.E. Miller, L. Carrillo-Reid, E. Pnevmatikakis, L. Paninski, R Yuste, and D.S. Peterka, *Neuron* **89**, 269-284 (2016).
- [37] S. Bovetti, C. Moretti, S. Zucca, M. Dal Maschio, P. Bonifazi, and T. Fellin. *Sci. Rep.* **7**, 40041 (2017).

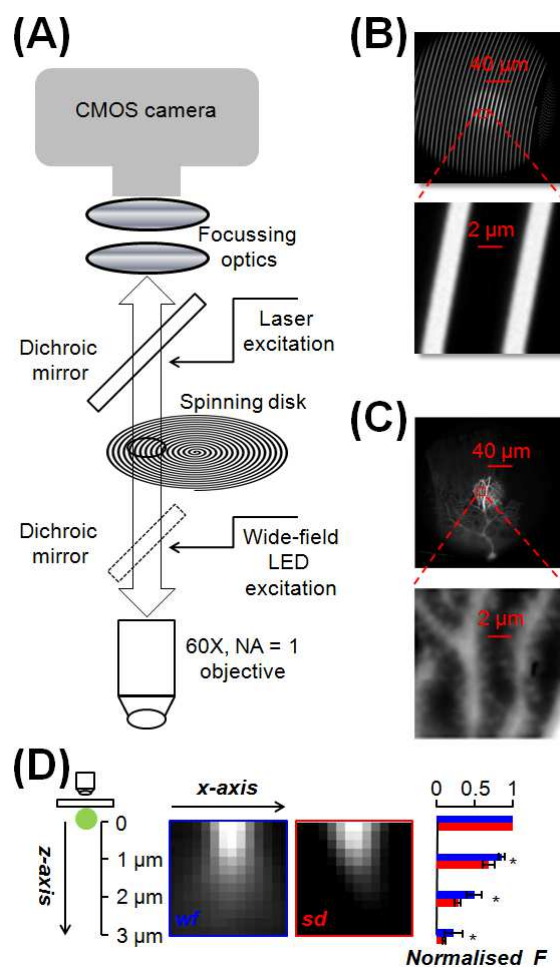


**Figure 1** Description of the confocal system. **(A)** Schematic showing a fast (20,000 rpm) spiral pattern spinning disk, coupled to a 465 nm multimode laser and fast CMOS camera. The configuration includes widefield LED illumination at 470 nm independent of the spinning disk. **(B)** Top: image of the disk obtained using a uniform fluorescence slide with the 60X objective. A frame obtained with whole-field LED illumination is superimposed to a frame with  $\sim 60 \mu\text{m}$  laser spot. Bottom: enlargement of the red square region on the top to appreciate the fine structure of the disk. **(C)** Top: image of a PN filled with OG5N showing the detailed confocal region acquired with laser and spinning disk superimposed over a full frame taken with widefield LED illumination. Bottom: enlargement of the red square region on the top to appreciate the resolution of dendrites and synaptic spines. **(D)** A 500 nm fluorescent bead attached to a coverslip is imaged at

different depths with 250 nm steps from its focal plane in widefield (*wf*) or with the spinning disk (*sd*); the two images are in the *xz* plane; on the right the mean  $\pm$  SD from  $N = 16$  beads of the fluorescence normalised to that in the focal plane at 1  $\mu\text{m}$ , 2  $\mu\text{m}$  and 3  $\mu\text{m}$  from the focal plane; \* indicates that the difference between *sd* and *wf* imaging was significantly different ( $p < 0.001$ , paired t-test)

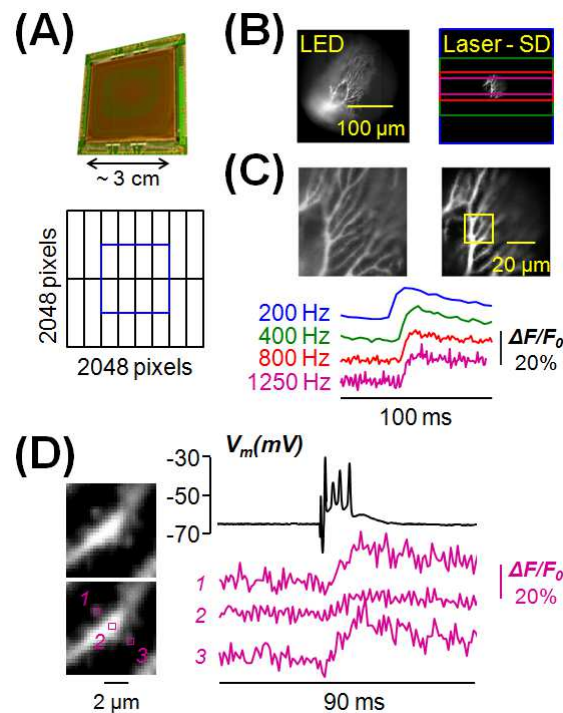


**Figure 2** Speed performance of the system. (A) Top: picture of the full CMOS sensor composed of 2048 x 2048 pixels of 15  $\mu\text{m}$  X 15  $\mu\text{m}$  (~3 cm length). Bottom: scheme of the 16 parallel processed sectors with blue square indicating the actual field of view. (B) Images of a PN filled with OG5N obtained with widefield LED illumination (left) and laser and spinning disk (right); in the image on the right, the blue, green, red and purple rectangles are CMOS areas where acquisitions can be achieved at maximal speeds of 200, 400, 800 and 1250 frames/s. (C) Top: image detail (160X160 pixels) obtained with

widefield LED illumination (left) and laser and spinning disk (right); Bottom:  $\text{Ca}^{2+}$  signals (single trials) associated with a CF-EPSP at the maximal speeds of the four rectangles in the yellow region on the top-right image. **(D)** Left: detail of the image in (C) with regions (2X2 pixels,  $\sim 0.25 \mu\text{m}^2$ ) 1 and 3 corresponding to synaptic spines and 3 in the parent dendrite. Right:  $\text{Ca}^{2+}$  signals (average of 3 trials) associated with a CF-EPSP in regions 1-3; somatic patch recording on the top.

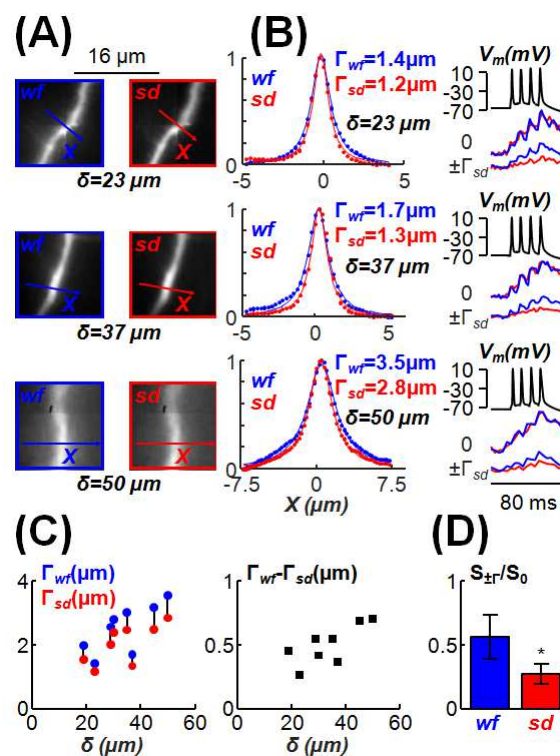


**Figure 3** Improvement of spinning disk (*sd*) imaging with respect of widefield (*wf*) imaging at different depths from the slice surface ( $\delta$ ). **(A)** Images of three apical dendrites from CA1 hippocampal pyramidal neurons at  $\delta = 23, 37$  or  $50 \mu\text{m}$  with *wf* imaging (blue, left) or with *sd* imaging (red, right); the X axes of analysis are positioned on the dendritic part in focus. **(B)** Left: fluorescence normalised to the maximum (at  $X = 0$ ) along the X axes (points) fitted with a Lorentzian functions (lines) in the three cases with *wf* and *sd* imaging; each spot was calculated by averaging fluorescence of 2X4 pixels;  $\Gamma$  values are

indicated. Right:  $\text{Ca}^{2+}$  signals (average of 4 trials) associated with 4 action potentials at 10 ms interval at  $X = 0$  and  $X = \pm\Gamma_{sd}$ ; since the *sd* is removing scattered light, the  $\text{Ca}^{2+}$   $\Delta F/F_0$  signal drops away more rapidly with distance from the dendritic centre making confocal imaging significantly better is resolving the origin of a  $\text{Ca}^{2+}$  signal. (C)  $\Gamma$  values with *wf* and *sd* imaging (left plot) and their difference (right plot) versus  $\delta$  in 8 X-lines from 5 cells. (D) Mean  $\pm$  SD of  $\text{Ca}^{2+}$   $\Delta F/F_0$  signal associated with 4 action potentials at  $X = \pm\Gamma$ , normalised to the signal at  $X = 0$ , in 8 X lines from 5 cells; \* indicates that the *sd* signal was significantly smaller than the *wf* signal ( $p < 0.001$ , paired t-test).

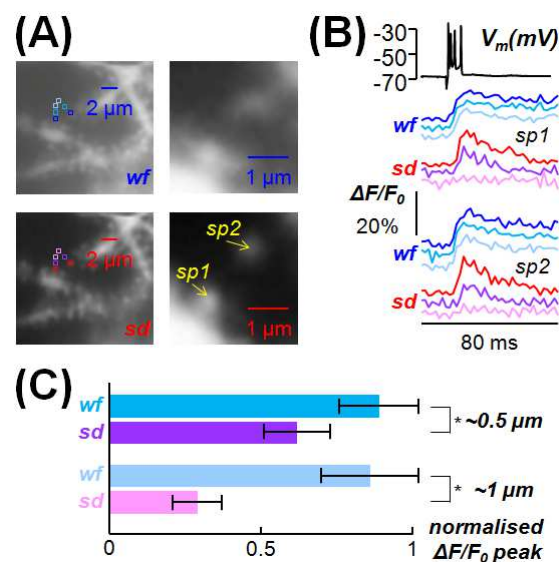


**Figure 4** Ability of the system to resolve  $\text{Ca}^{2+}$  transients from synaptic spines. (A) Images of a PN dendrite at  $\delta = 25 \mu\text{m}$  with widefield illumination (*wf*, top) or with the spinning disk (*sd*, bottom); two spines in focus (*sp1* and *sp2*) are indicated on the right; 2X2 pixels regions centred on *sp1* and *sp2*, at  $\sim 0.5 \mu\text{m}$  from the spine or at  $\sim 1 \mu\text{m}$  from the spine are shown on the left. (B)  $\text{Ca}^{2+}$  signals (average of 8 trials) associated with a CF-EPSP at 500 Hz in the regions in (A) shown in the same colour code; somatic patch recording on the top; the  $\text{Ca}^{2+}$   $\Delta F/F_0$  signal decreases with distance in *sd* imaging but not in *wf* imaging. (C) Mean  $\pm$  SD of  $\text{Ca}^{2+}$   $\Delta F/F_0$  signal associated with a CF-EPSP,

normalised to the signal in the spines, from 2 x 2 pixels regions at  $\sim 0.5 \mu\text{m}$  from the spine or at  $\sim 1 \mu\text{m}$  from the spine calculated over 48 spines in focus in six cells with  $\delta$  ranging from  $18 \mu\text{m}$  to  $30 \mu\text{m}$ ; \* indicates that both at  $\sim 0.5 \mu\text{m}$  and at  $\sim 1 \mu\text{m}$  the difference between *sd* and *wf* imaging was significantly different ( $p < 0.001$ , paired t-test)

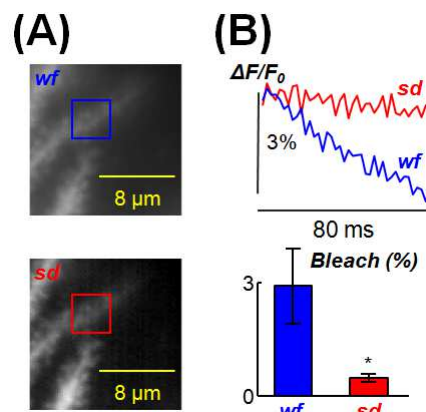


**Figure 5** Bleach improvement of the system. (A) Images of a PN dendrite detail with widefield illumination (*wf*, top) or with the spinning disk (*sd*, bottom); a region of interest is indicated. (B) Top:  $\Delta F/F_0$  from the region of interest in *wf* (blue trace) and *sd* (red trace) mode following 80 ms light application; light intensity was the maximum for the *sd* whereas it was decreased in *wf* in order to obtain comparable photon noise. Bottom: mean  $\pm$  SD of the  $\Delta F/F_0$  in *wf* and *sd* (red trace) mode following 80 ms light application, calculated from  $N = 7$  cells; \* indicates that the difference between *sd* and *wf* imaging was significantly different ( $p < 0.001$ , paired t-test)

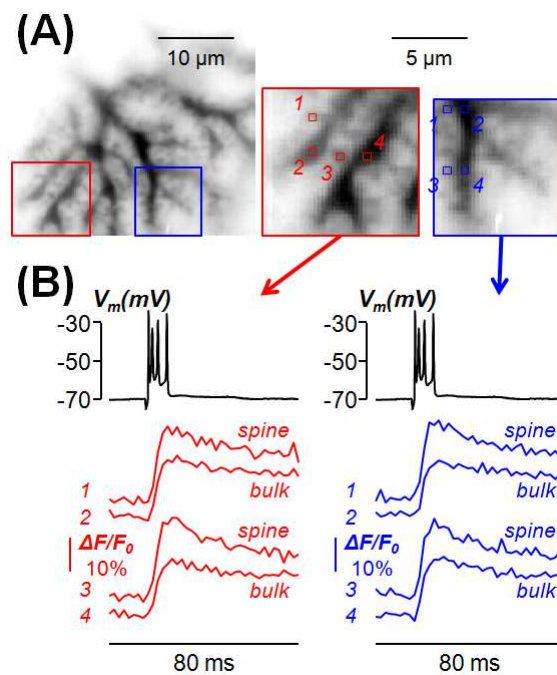


**Figure 6** Example 1: analysis of  $\text{Ca}^{2+}$  transients associated with a CF-EPSP. (A) Left: intensity inverted confocal image of a PN filled with OG5N. Right: enlargements of the red and blue square regions of the left with four spine regions (1 and 3) and four regions of the parent dendrites (2 and 4). (B)  $\text{Ca}^{2+}$  signals (average of 8 trials) associated with a CF-EPSP at 500 Hz in the spines and dendritic regions in (A); somatic patch recording on the top. For this experiment, see also MovieS1.

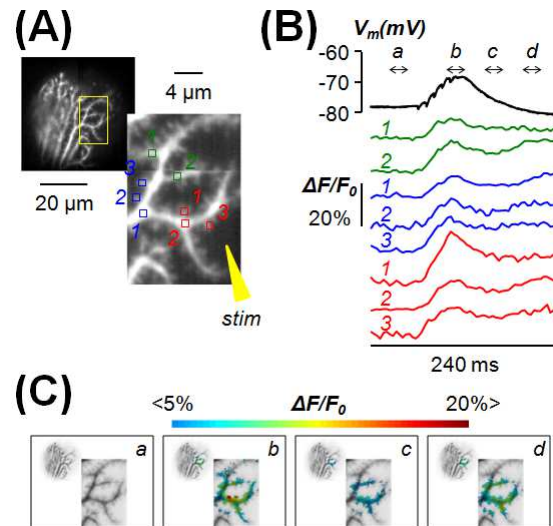


**Figure 7** Example 2: analysis of  $\text{Ca}^{2+}$  transients associated with parallel fibre EPSPs. **(A)** Left: confocal image of a PN filled with OG5N. Right: enlargements of the activated dendritic region with 8 spine or dendritic regions indicated. **(B)**  $\text{Ca}^{2+}$  signals (average of 8 trials) associated with a train of 5 parallel fibre EPSPs at 250 Hz in the spines and dendritic regions in **(A)**; somatic patch recording on the top. **(C)** Colour scaled signals of the experiment in **(B)** superimposed on the inverted fluorescence image of the dendrite. Signal profiles are obtained by averaging 6 frames in the time windows *a*, *b*, *c* and *d* indicated in **(B)**. Signal *b* corresponds to the peak of the fast component of the  $\text{Ca}^{2+}$  transient, mediated by voltage-gated  $\text{Ca}^{2+}$  channels. Signal *d* corresponds to the peak of the slow component of the  $\text{Ca}^{2+}$  transient, mediated by metabotropic glutamate receptors. For this experiment see also MovieS2.